Theoretical Study on the Reaction of Tropospheric Interest: Hydroxyacetone + OH. Mechanism and Kinetics

ARTICLE *in* THE JOURNAL OF PHYSICAL CHEMISTRY A · AUGUST 2006

Impact Factor: 2.69 · DOI: 10.1021/jp061705b · Source: PubMed

1 AUTHOR:

Annia Galano
Metropolitan Autonomous University
153 PUBLICATIONS **3,362** CITATIONS

SEE PROFILE

Theoretical Study on the Reaction of Tropospheric Interest: Hydroxyacetone + OH. Mechanism and Kinetics

Annia Galano*

Instituto Mexicano del Petróleo, Eje Central Lázaro Cárdenas 152, 007730 México DF, México

Received: March 19, 2006; In Final Form: May 31, 2006

A theoretical study of the mechanism and kinetics of the OH hydrogen abstraction from hydroxyacetone is presented. Optimum geometries and frequencies have been computed at the BHandHLYP/6-311++G(d,p) level of theory for all stationary points. Energy values have been improved by single-point calculations at the above geometries using CCSD(T)/ 6-311++G(d,p). The rate coefficients are calculated for the temperature range 280−500 K by using conventional transition state theory (TST), including tunneling corrections. Our analysis supports a stepwise mechanism involving the formation of a reactant complex in the entrance channel and a product complex in the exit channel, for all the modeled paths. Four experimental values of the rate constant at 298 K have been previously reported: three of them in great agreement ($\sim 3 \times 10^{-12}$ cm^3 molecule^{-1} s^{-1}), and one of them twice larger. The calculations in the present work support the smaller value. A curved Arrhenius plot was found in the studied temperature range; thus the expression that best describes the obtained data is $k_{\text{overall}}^{280-500} = 5.29 \times 10^{-23} T^{3.4} e^{1623/T}$ cm^3 molecule^{-1} s^{-1}. The activation energy was found to vary with temperature from −1.33 to +0.15 kcal/mol.

Introduction

The tropospheric oxidation of dienes leads to the production of multifunctional oxygenated species, which can be highly reactive themselves. Thus, the elucidation of the oxidation rates and mechanisms for these oxygenated species is crucial to the assessment of the overall environmental impact of dienes emissions. Some of these species are hydroxyacetone ($HOCH_2$-CHO), methylglyoxal ($CH_3C(O)CHO$), and hydroxyacetone ($HOCH_2C(O)CH_3$),[1,2] which arise from the isoprene oxidation. Unfortunately, there are rather scarce data available in the literature dealing with the tropospheric fate of such compounds.[3] In recent works our group has investigated the reactions of glycolaldehyde,[4] glyoxal and methylglyoxal[5] with hydroxyl radicals. It is the aim of the present work to study in detail the mechanism and kinetics of the gas-phase reaction of hydroxyacetone + OH, which is expected to be the main sink of this compound in the troposphere. Recent measurements of hydroxyacetone concentrations in the free and upper troposphere[6] indicate that the reactions of this compound can be relevant to the tropospheric chemistry.

Dagaut et al.[7] determined the absolute rate constant of the OH radical toward hydroxyacetone at 298 K using the flash photolysis resonance fluorescence technique. They reported a rate constant of $(3.01 \pm 0.30) \times 10^{-12}$ cm^3 molecule^{-1} s^{-1} for the overall reaction, leading to a tropospheric lifetime of about 4 days. Orlando et al.[8] reported a value of $(3.0 \pm 0.7) \times 10^{-12}$ cm^3 molecule^{-1} s^{-1} using a relative rate technique with methanol and ethanol as references and FTIR spectroscopic method. Chowdhury et al.[9] have reported a value of $(2.8 \pm 0.2) \times 10^{-12}$ cm^3 molecule^{-1} s^{-1}, determined by the laser induced fluorescence technique. While this work was in preparation, Dillon et al.[10] reported a rate coefficient that is about twice those corresponding to previous measurements [$(5.95 \pm 0.5) \times 10^{-12}$ cm^3 molecule^{-1} s^{-1}]. The authors also report a temperature dependence within the range 233−363 K of $(2.15 \pm 0.30) \times 10^{-12} e^{(305 \pm 10)/T}$ cm^3 molecule^{-1} s^{-1}.

The methodology used in the present work has been successfully used to quantitatively describe the kinetics and mechanism of gas-phase hydrogen abstraction reactions from diverse volatile organic compounds.[4,5,11−17] The excellent agreement between the calculated and experimental results obtained for such a wide range of reactions supports the reliability of the method. In the current work, each abstraction path of the hydroxyacetone + OH reaction has been modeled as a complex mechanism involving the formation of a reactant complex in the entrance channel and a product complex in the exit channel. Recent theoretical studies[18−23] have proposed that oxygenated and unsaturated compounds react with OH radicals through a complex mechanism, involving a reactant complex. The role of these intermediates in bimolecular reactions has been recently reviewed.[24] Reactant complexes involving the OH radical have also been studied experimentally.[25,26] Moreover, it has been established that the presence of an attractive well at the entrance channel of a potential energy surface can influence the dynamics, and hence the course of the reaction.[24] The existence of a reactant complex can manifest itself in terms of negative temperature dependence, which is to be expected when there is an attractive encounter between reactants. The role of such complexes has been recently pointed out for the OH reaction with acetone and acetaldehyde,[27] which shows curved Arrhenius plots and negative temperature dependence.

The aim of this work is to study in detail the OH radical reaction with hydroxyacetone, by assuming that it occurs according to a complex mechanism that involves a barrierless first step that leads to the formation of a thermally stabilized reactant complex. In the second step, an energy barrier that is higher than the apparent activation energy leads to the formation of a product complex, and then to the corresponding radical and water. A description of the temperature dependence of the hydroxyacetone + OH reaction is given.

10.1021/jp061705b CCC: $33.50
Published on Web 07/01/2006

In addition, a conformational study of hydroxyacetone has been performed, and the relative population of the most stable conformers has been taken into account in the calculation of the overall rate constant.

The results reported here are relevant to the understanding of the tropospheric chemistry of hydroxyacetone and to the assessment of its importance as a secondary pollutant. In addition, our calculations provide additional information on the kinetics of a reaction for which some disagreements among the experimental data have been reported.

Computational Details

Five stationary points have been modeled along each reaction path: the isolated reactants, the reactant complex, the transition state, the product complex and the products. Full geometry optimizations were performed with the Gaussian 98[28] program using the BHandHLYP hybrid HF-density functional and the 6-311++G(d,p) basis set. The energies of all the stationary points were improved by single point calculations at the CCSD(T)/6-311++G(d,p) level of theory. Unrestricted calculations were used for open shell systems. Frequency calculations were carried out for all the stationary points at the DFT level of theory and local minima and transition states were identified by the number of imaginary frequencies (NIMAG = 0 or 1, respectively). Intrinsic reaction coordinate (IRC) calculations were carried out at the BHandHLYP/6-311G++(d,p) level of theory to confirm that the transition states structures do connect the proper reactants and products. Zero point energies (ZPE) and thermal corrections to the energy (TCE) at 298.15 K were included in the determination of the activation energies and of the heats of reaction, respectively.

The conventional transition state theory (TST)[29,30] implemented in the Rate 1.1 program,[31] was used to calculate the rate coefficients because it has the advantage of being inexpensive for a high level of ab initio calculations. The tunneling correction defined as the Boltzmannn average of the ratio of the quantum and the classical probabilities were calculated using the Eckart method.[32] This method approximates the potential by a one-dimensional function that is fitted to reproduce the zero-point energy corrected barrier, the enthalpy of reaction at 0 K, and the curvature of the potential curve at the transition state. This method tends to overestimate the tunneling contribution, especially at very low temperature, because the fitted Eckart function is often too narrow. However, sometimes it compensates for the corner-cutting effect not included in the Eckart approach.[33−35] Such compensation can lead to Eckart transmission coefficients similar[34] or even lower[35] than those obtained by the small-curvature tunneling (SCT) method[36] at temperatures equal to or higher than 300 K. In addition, in this work, the partition function values have been corrected by replacing some of the large amplitude vibrations by the corresponding hindered internal rotations, when necessary.

Results and Discussion

Geometries. Hydroxyacetone has three internal rotational degrees of freedom: the CH_3-CO (ϕ_1), $CO-CH_2$ (ϕ_2) and $HO-CH_2$ (ϕ_3) bond torsions (Figure 1). Several different minima were fully optimized at the BHandHLYP/6-311++G(d,p) level of calculation and the two most stable conformations will be the only ones considered in this work. They correspond to the OO-*s*-cis and OO-*s*-trans isomers and their contributions to the total population at 298 K are 94% and 6%, respectively. Structure I (Figure 1) is stabilized by an intramolecular hydrogen bond between the carbonyl oxygen and the hydroxyl hydrogen at 2.056 Å.

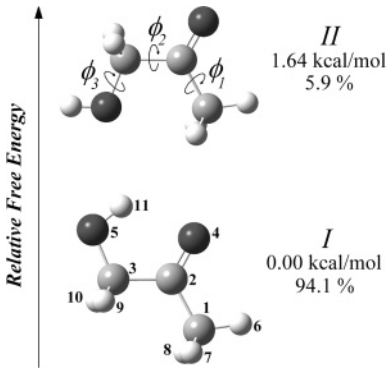

Figure 1. Fully optimized BHandHLYP/6-311++G(d,p) hydroxyacetone conformers.

Three reaction channels have been modeled for both conformers I and II:

$$HOCH_2C(O)CH_3 + OH \rightarrow HOCH_2C(O)CH_2 + H_2O \quad (a)$$

$$\rightarrow HOCHC(O)CH_3 + H_2O \quad (b)$$

$$\rightarrow OCH_2C(O)CH_3 + H_2O \quad (c)$$

Each of them consists of three steps, namely, (1) the formation or the reactant complex from the isolated reactants, (2) the formation of the product complex from the reactant complex and (3) the formation of the corresponding radical and water from the product complex:

$$HK + OH \underset{(-1)}{\overset{(1)}{\rightleftharpoons}} RC \xrightarrow{(2)} PC \underset{(-3)}{\overset{(3)}{\rightleftharpoons}} R + H_2O$$

where H represents hydroxyacetone and RC, PC and R represent the reactant complex, product complex and radical product corresponding to each particular path.

Each a channel was modeled by taking into account the conformation of the abstracted H atom. Taking the carbonyl group as reference, two possible orientations have been considered corresponding to abstractions from the methyl group. This differentiation has been previously applied for ketones + OH reactions.[17,37] The two conformations are:

Eclipsed: The hydrogen atom is in the eclipsed conformation with respect to the carbonyl group

Alternated: The dihedral angle between the hydrogen to be abstracted and the oxygen atom in the carbonyl group is about +120 or −120°.

Bader topological analyses[38,39] have been performed, for the BHandHLYP/6-311++G(d,p) wave functions of different stationary points, to characterize the interactions between nonbonded atoms. This kind of analysis provides electronic charge density $\rho(r)$ and its Laplacian, $\nabla^2\rho(r)$. The critical points of $\rho(r)$, which present two negative curvatures and one positive curvature, identify the bonds in the molecule and will be denoted hereafter as bond critical points (BCP). The critical points with one negative and two positive curvatures are associated with the existence of a ring structure and will be denoted as ring critical points (RCP). The values of $\rho(r)$ and $\nabla^2\rho(r)$ at these points provide quantitative information on the strength and nature of the bonding and the characteristics of the ring. The Laplacian of the electronic charge density, $\nabla^2\rho(r)$, identifies regions of space wherein $\rho(r)$ is locally concentrated, $\nabla^2\rho(r) < 0$, or depleted, $\nabla^2\rho(r) > 0$. In general, negative values of $\nabla^2\rho(r)$ are typical of covalent interactions, whereas interactions between closed-shell systems are characterized by positive values of $\nabla^2\rho(r)$.

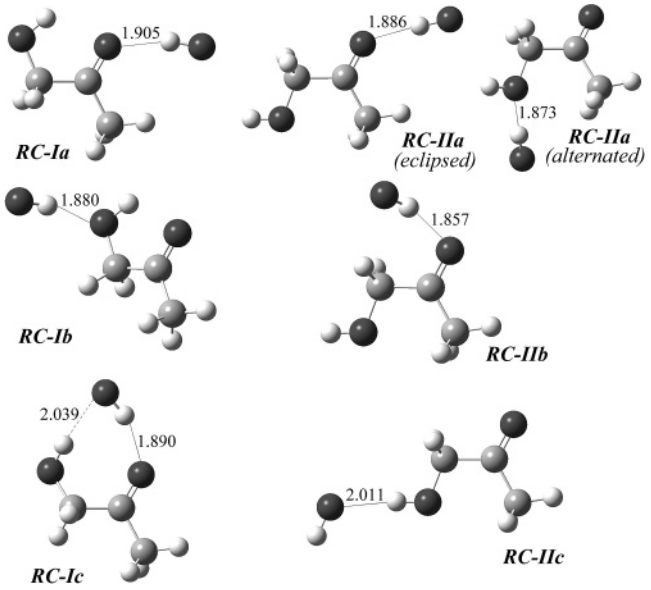

Figure 2. Fully optimized BHandHLYP/6-311++G(d,p) reactant complexes of the hydroxyacetone + OH reaction.

In all, seven reactant complexes were identified (Figure 2), because the alternated conformation corresponding to channel Ia evolved toward the eclipsed one during the geometry optimization process. The reactant complex corresponding to abstraction from the $-CH_3$ group in conformer I (RC-Ia) is stabilized by the attractive interaction between H in the OH radical and the O atom in the carbonyl group, at a distance (d) of 1.905 Å. The reactant complex corresponding to abstraction from $-CH_2$ in conformer I (RC-Ib) is caused by the attractive interaction between H in the OH radical and the O atom in the hydroxyl group, at a distance $d_{5-13} = 1.880$ Å. Two attractive interactions are responsible for the formation of the RC corresponding to abstraction from $-$OH group in conformer I (RC-Ic). The main one occurs between the H atom in the OH radical and the O in the carbonyl group, with $d_{4-13} = 1.890$ Å. The other one, between O in the OH radical and H in the hydroxyl group has $d_{11-12} = 2.039$ Å. The presence of these interactions causes the reactant complex to form a ring-like structure. The electronic charge density (ρ) and its Laplacian, $\nabla^2\rho(r)$, at the critical points are reported in Table 1.

Four reactant complexes were found for conformer II (Figure 2). RC-IIa, eclipsed and alternated, correspond to hydrogen abstraction from the methyl group. RC-IIa (eclipsed) is formed due to the interaction between the H atom in the OH radical and the O atom in the carbonyl group, at a distance $d_{4-13} =$ 1.886 Å. The RC-IIa (alternated) is formed due to the interaction between the H atom in the OH radical and the O atom in the hydroxyl group, at a distance $d_{5-13} = 1.873$ Å. The RC corresponding to H abstraction from the $-CH_2$ group (RC-IIb) is caused by the same interaction as for RC-IIa, with $d_{4-13} =$ 1.857 Å. RC-IIc corresponds to H abstraction from the hydroxyl group in conformer II and is caused by the interaction between O in the OH radical and H in the hydroxyl group.

All the transition state (TS) structures considered in this work are shown in Figure 3. In all, seven transition states were identified (Figure 2). The TS structure corresponding to abstractions of the alternated H in the CH_3 group of OO-*s*-cis hydroxyacetone evolved toward the eclipsed one during the geometry optimization process. Accordingly, two TS structures were identified for channel IIa and only one for channel Ia. The main structural change associated with the formation of the TS corresponding to H abstraction from the methyl group

TABLE 1: Electronic Charge Density (ρ) and Its Laplacian, $\nabla^2\rho(r)$, for Critical Points Involving Nonbonded Atoms[a]

		atoms	ρ	$\nabla^2\rho(r)$
RC-Ia	BCP	4, 13	0.0260	−0.0250
RC-Ib	BCP	5, 13	0.0281	−0.0267
RC-Ic	BCP	4, 13	0.0274	−0.0262
	BCP	11, 12	0.0199	−0.0184
	RCP	2−5, 11−13	0.0091	−0.0094
RC-IIa, eclipsed	BCP	4, 13	0.0260	−0.0261
RC-IIa, alternated	BCP	5, 13	0.0277	−0.0273
RC-IIb	BCP	4, 13	0.0272	−0.0258
RC-IIc	BCP	11, 12	0.0197	−0.0199
TS-Ic	BCP	4, 13	0.0199	−0.0186
	RCP	2−5, 11−13	0.0106	−0.0124
TS-IIa, eclipsed	BCP	4, 13	0.0148	−0.0131
	RCP	1, 2, 4, 6, 12, 13	0.0125	−0.0145
TS-IIa, alternated	BCP	5, 13	0.0174	−0.0166
	RCP	1−3, 5, 7, 12, 13	0.0096	−0.0111
PC-Ia	BCP	4, 13	0.0144	−0.0148
PC-Ib	BCP	5, 13	0.0164	−0.0154
PC-Ic	BCP	4, 13	0.0175	−0.0173
	BCP	10, 12	0.0073	−0.0068
	RCP	2−4, 10−12	0.0068	−0.0072
PC-IIa, eclipsed	BCP	4, 13	0.0250	−0.0244
	BCP	7, 12	0.0089	−0.0090
	RCP	1, 2, 4, 7, 12, 13	0.0069	−0.0084
PC-IIa, alternated	BCP	5, 13	0.0231	−0.0244
	BCP	8, 12	0.0112	−0.0104
	RCP	1−3, 5, 8, 12, 13	0.0074	−0.0078
PC-IIb	BCP	4, 13	0.0272	−0.0260
	BCP	9, 12	0.0108	−0.0114
	RCP	2−4, 9, 12, 13	0.0077	−0.0095
PC-IIc	BCP	5, 11	0.0164	−0.0167
	BCP	8, 12	0.0095	−0.0082
	RCP	1−3, 5, 8, 11, 12	0.0048	−0.0055

[a] For the atoms numbering, see Figure 1.

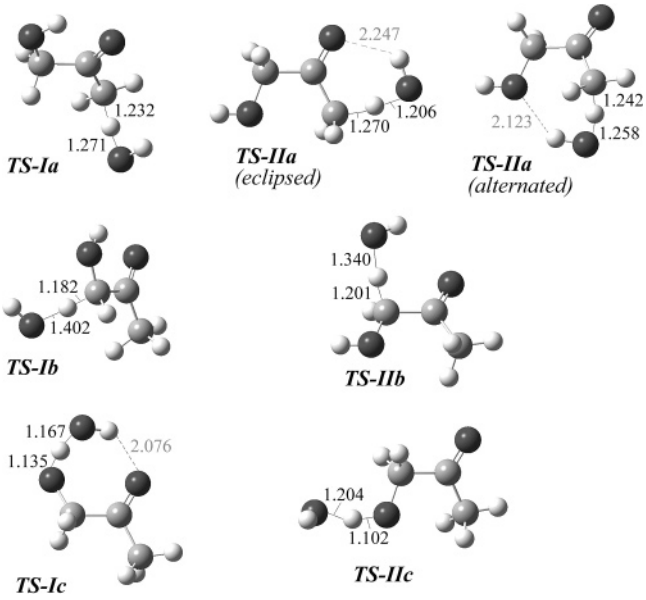

Figure 3. Fully optimized BHandHLYP/6-311++G(d,p) transition states of the hydroxyacetone + OH reaction.

in the OO-*s*-cis conformer (TS-Ia) is an elongation of d_{1-6} by 0.15 Å, compared to that for free hydroxyacetone. Another minor variation observed in TS-Ia with respect to the reactant is the shortening of the C1C2 bond by 0.015 Å. The attack of the OH radical was found to be almost collinear, with the C1H6O12 angle equal to 173.1°. TS-Ib in Figure 3 corresponds to abstraction from the $-CH_2$ group in conformer I. It shows an elongation in d_{3-9} of 0.091 Å compared to that for the free reactant, and slight shortening of distances d_{3-5} and d_{2-3}, by

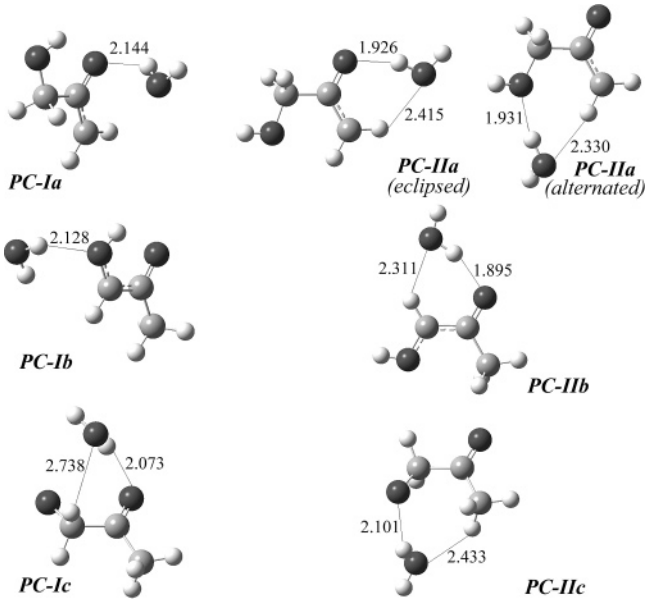

Figure 4. Fully optimized BHandHLYP/6-311++G(d,p) product complexes of the hydroxyacetone + OH reaction.

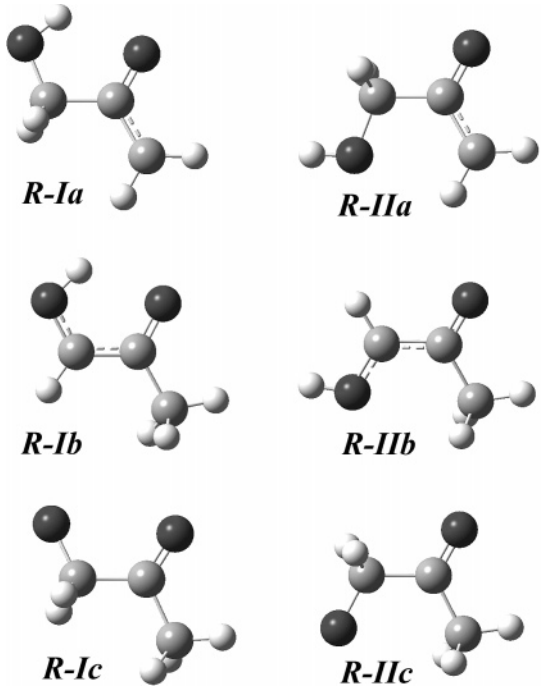

Figure 5. Fully optimized BHandHLYP/6-311++G(d,p) radical products of the hydroxyacetone + OH reaction.

0.023 and 0.004 Å, respectively. The OH attack was found to be collinear, with a C3H9O12 angle of 178.7°. The transition state corresponding to channel *c* in conformer I (TS-Ic) shows an elongation of 0.178 Å in the O5H11 bond and a shortening of 0.011 Å in the C3O5 bond. A stabilizing intramolecular hydrogen bond was found between H in the OH fragment and the carbonylic O in the hydroxyacetone fragment, with $d_{4-11} = 2.076$ Å.

The TSs corresponding to abstraction from $-CH_3$ {TS-IIa (eclipsed) and TS-IIa (alternated)}, as well as from $-CH_2$ (TS-IIb), and $-OH$ (TS-IIc) groups in conformer II, are also shown in Figure 3. The main structural changes associated with the formation of the transition structures associated to abstraction from the methyl group are the elongations of d_{1-6} and d_{1-7} by 0.188 and 0.156 Å, for the eclipsed and alternated forms, respectively. Other minor variations with respect to free OO-*s*-tans hydroxyacetone are the shortening of the C1C2 bond by 0.005 Å (eclipsed) and 0.015 Å (alternated). The attack of the OH radical was found to be noncollinear, with the C1H6O12 and C1H7O12 angles being equal to 165°. Both TS-IIa show ring-like structures, caused by intramolecular interactions, which have been characterized by Bader's topological analysis (Table 1). TS-IIb shows a C3H10 bond elongation of 0.112 Å compared to that for the free reactant, and slight shortenings of 0.010 and 0.028 for distances of d_{2-3} and d_{3-5}, respectively. The OH attack was found to be noncollinear, with a C3H10O12 angle of 167.8°. TS-IIc shows an elongation of 0.152 Å in the O5H11 bond and a shortening of 0.015 Å in the C3O5 bond.

The seven product complexes (PC) corresponding to all the computed paths have been also modeled and fully optimized (Figure 4). The product complex corresponding to the abstraction from the $-CH_3$ group in conformer I (PC-Ia) is formed due to the attractive interaction between an H in the water molecule and the O atom in the carbonyl group, with an interaction distance of 2.144 Å. The product complex corresponding to abstraction from $-CH_2$ in conformer I (PC-Ib) is caused by an attractive interactions between one H in the water molecule and the O atom in the hydroxyl group, with $d_{5-13} = 2.128$ Å. The formation of the PC corresponding to abstraction from the $-OH$ in conformer I (PC-Ic) can be attributed to two attractive interactions. The main one occurs between one H atom in the water molecule and the O in the carbonyl group, with $d_{4-13} = 2.073$ Å. The other one, between the O in the water molecule and one of the H in the CH_2 group has $d_{10-12} = 2.738$ Å.

The product complexes corresponding to H abstractions from conformer II are also shown in Figure 4, all of them were found to be caused by two attractive interactions. Accordingly, all the product complexes show ring-like structures. PC-IIa (eclipsed) shows the main one between one H atom in the water molecule and the O atom in the carbonyl group, with $d_{4-13} = 1.926$ Å and the weaker one with $d_{7-12} = 2.415$ Å. The stronger interaction in the PC-IIa (alternated) complex was found to be between one H atom in the water molecule and the O atom in the hydroxyl group, with $d_{5-13} = 1.931$ Å, and the weaker one with $d_{7-12} = 2.330$ Å. PC-IIb and PC-IIc show interaction distances of 1.895 and 2.311 Å; and 2.101 and 2.433 Å, respectively. Values of electronic charge density and its Laplacian, characterizing all the described interactions are reported in Table 1.

The radical products corresponding to all the abstraction paths from both conformers are shown in Figure 5. Their geometries remain nearly unchanged, compared to those of the corresponding product complexes.

Energies. The energies of all the modeled stationary points, relative to the isolated reactants, are shown in Table 2 and Figure 6. They show that all the studied stationary points are lower in energy than the corresponding reactants, with the exception of the transition states corresponding to channels Ia, Ic, IIa and IIc. Therefore, negative overall energy barriers ($E_{overall} = E_{TS} - \Sigma E_{reactants}$) are observed for the H abstractions from the $-CH_2$ group in both conformers. The stabilization energies of the reactant complexes ($E_{RC} - E_{React}$) are larger than 4 kcal/mol for all the modeled abstractions, which supports the complex mechanism assumption. The presence of the reactant complexes explains the $E_{overall}$ negative sign and leads to the following adiabatic effective barriers ($E_{eff} = E_{TS} - E_{RC}$): E_{eff}(Ia) = 8.07, E_{eff}(Ib) = 3.53, E_{eff}(Ic) = 8.40, E_{eff}(IIa,eclipsed) = 8.27, E_{eff}(IIa,alternated) = 6.20, E_{eff}(IIb) = 4.01 and E_{eff}(IIc) = 7.09 kcal/mol. These values show that for both conformers the lowest

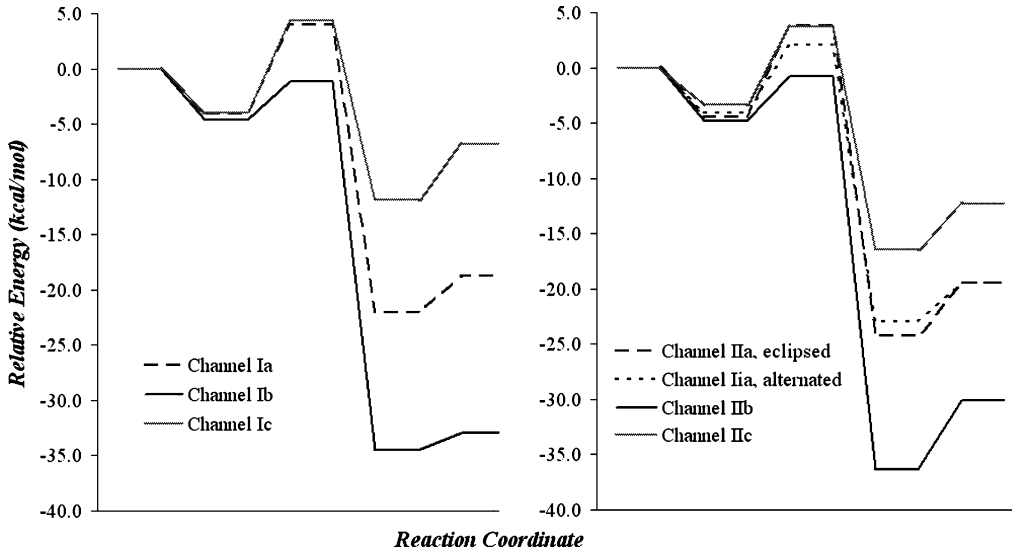

Figure 6. Reaction profiles at CCSD(T)//BHandHLYP/6-311++G(d,p) level of theory.

TABLE 2: CCSD(T)//BHandHLYP/6-311++G(d,p) Adiabatic Energies (kcal/mol) Relative to the Isolated Reactants

conformer I		conformer II	
RC-Ia[a]	−4.11	RC-IIa[a] eclipsed	−4.44
		alternated	−4.10
RC-Ib[a]	−4.63	RC-IIb[a]	−4.77
RC-Ic[a]	−4.03	RC-IIc[a]	−3.35
TS-Ia[a]	3.96	TS-IIa[a] eclipsed	3.83
		alternated	2.10
TS-Ib[a]	−1.10	TS-IIb[a]	−0.77
TS-Ic[a]	4.37	TS-IIc[a]	3.74
PC-Ia[b]	−21.30	PC-IIa[b] eclipsed	−23.80
		alternated	−23.06
PC-Ib[b]	−33.79	PC-IIb[b]	−36.44
PC-Ic[b]	−10.83	PC-IIc[b]	−15.99
R-Ia + H_2O[b]	−18.22	R-IIa + H_2O[b]	−19.45
R-Ib + H_2O[b]	−32.90	R-IIb + H_2O[b]	−30.00
R-Ic + H_2O[b]	−6.11	R-IIc + H_2O[b]	−12.64

[a] Including ZPE corrections. [b] Including TCE corrections at 298 K.

effective barriers, of the second elementary step, correspond to H abstractions from the $-CH_2$ group. These values also support the use of conventional TST for the kinetic studies, because they are large enough to prevent significant recrossing effects.

Rate Coefficients. According to the shape of the reaction profiles, the rate coefficients (k) corresponding to all the studied reaction channels can be analyzed in terms of conventional TST. Consistent with the reaction mechanism proposed above, if k_1 and k_{-1} are the forward and reverse rate constants for the first step and k_2 corresponds to the second step, a steady-state analysis leads to a rate coefficient for each overall reaction channel that can be written as

$$k = \frac{k_1 k_2}{k_{-1} + k_2} \tag{1}$$

Even though when the energy barrier for k_{-1} is about the same size as that for k_2, the entropy change is much larger in the reverse reaction than in the formation of the products. The activation entropy ΔS_2 is small and negative because the transition state structure is tighter than the reactant complex, whereas ΔS_{-1} is large and positive because six vibrational degrees of freedom are converted into three translational plus three rotational degrees of freedom. Analyzing channel Ib, for instance, the barrier for step 2 is 0.71 kcal lower than the barrier for step −1; however, the entropy changes are $\Delta S_2 = -1.18$ and $\Delta S_{-1} = 5.37$ kcal/mol, which overcome the difference in barrier heights; i.e., ΔG_{-1} is 5.85 kcal/mol lower than ΔG_2, which makes k_{-1} about 4 orders higher than k_2. On the basis of this assumption, first considered by Singleton and Cvetanovic,[40] k can be rewritten as

$$k = \frac{k_1 k_2}{k_{-1}} = K_{eq} k_2 \tag{2}$$

where K_{eq} is the equilibrium constant between the isolated reactants and the reactant complex and k_2 is the rate constant corresponding to the second step of the mechanism, i.e., transformation of the reactant complex into products.

Applying basic statistical thermodynamic principles the equilibrium constant (k_1/k_{-1}) of the fast preequilibrium between the reactants and the reactant complex may be obtained as

$$K_{eq} = \frac{Q_{RC}}{Q_R} \exp[(E_R - E_{RC})/RT] \tag{3}$$

where Q_{RC} and Q_R represent the partition functions corresponding to the reactant complex and the isolated reactants, respectively.

In a unimolecular process, under high-pressure conditions, an equilibrium distribution of reactants is established and the TST formula can be applied[41] to calculate k_2:

$$k_2 = \kappa_2 \frac{k_B T}{h} \frac{Q_{TS}}{Q_{RC}} \exp[(E_{RC} - E_{TS})/RT] \tag{4}$$

where κ_2 is the tunneling factor, k_B and h are the Boltzmann and Planck constants, respectively, and Q_{TS} is the transition state partition function. The energy difference includes the ZPE corrections. The effective rate coefficient of each channel is then obtained as

$$k = \sigma K_{eq} k_2 \tag{5}$$

where σ is the symmetry factor, which accounts for the number of equivalent reaction paths.

We have assumed that the reactant complex undergoes collisional stabilization, that is, the reaction occurs at the high

pressure limit. We have used this limit as our working hypothesis, because there is no experimental evidence that indicates otherwise. This approach has been previously used to describe OH radical reactions with several volatile organic compounds (VOCs). It is also adequate to account for the experimental negative activation energy observed for the hydroxyacetone + OH reaction. In a classical treatment the influence of the complex exactly cancels in eq 5 and the overall rate coefficient depends only on properties of OH, hydroxyacetone and the transition states. However, in the present case, there is a possibility of quantum mechanical tunneling, and the existence of the complex means that there are extra energy levels from where tunneling may occur so that the tunneling factor, κ, increases. We have assumed that a thermal equilibrium distribution of energy levels is maintained, which corresponds to the high-pressure limiting behavior. Thus, energy levels from the bottom of the well of the complex up to the barrier might contribute to tunneling.

It has been assumed that neither mixing nor crossover between different pathways occurs. Thus, the rate coefficient (k) corresponding to each conformer of hydroxyacetone + OH, is determined as the sum of the rate coefficients of each path:[42]

$$k_{\mathrm{I}} = k_{\mathrm{Ia}} + k_{\mathrm{Ib}} + k_{\mathrm{Ic}} \tag{6}$$

$$k_{\mathrm{II}} = k_{\mathrm{IIa}}^{\mathrm{eclipsed}} + k_{\mathrm{IIa}}^{\mathrm{alternated}} + k_{\mathrm{IIb}} + k_{\mathrm{IIc}} \tag{7}$$

In addition, the populations of both conformers have been taken into account; thus the overall rate coefficient, which measures the rate of OH disappearance, was calculated at each temperature as

$$k_{\mathrm{overall}} = p_{\mathrm{I}} k_{\mathrm{I}} + p_{\mathrm{II}} k_{\mathrm{II}} \tag{8}$$

where p_{I} and p_{II} account for the fractions of conformers I and II, respectively.

Because accurate rate constant calculations require the proper computation of the partition functions (Q), the hindered rotor approximation has been used to correct the Q's corresponding to internal rotations with torsional barriers comparable to RT. Direct inspection of the low-frequency modes of the studied stationary points indicates that there are several modes that correspond to hindered rotations. These modes should be treated as hindered rotors instead as vibrations.[43] To make this correction, these modes were removed from the vibrational partition function of the corresponding species and replaced with the hindered rotor partition function (Q^{HR}). In our calculations we have adopted the analytical approximation to Q^{HR} for a one-dimensional hindered internal rotation proposed by Ayala and Schlegel.[44]

The value of the overall rate coefficients at the studied temperatures are reported in Table 3, together with k_{I}, k_{II} and the fractions of both conformers. In this table the branching ratios corresponding to abstraction from the $-CH_3$ (Γa), $-CH_2$ (Γb) and $-OH$ (Γc) sites have also been included. They have been calculated as

$$\Gamma_{\mathrm{a,b\ or\ c}} = \frac{k_{\mathrm{a,b\ or\ c}}}{k_{\mathrm{overall}}} 100 \tag{9}$$

There is good agreement between the experimental and calculated values of k_{overall}, at 298 K. Differences between our value and those reported by Dagaut et al.,[7] Orlando et al.,[8] and Chowdhury et al.[9] are of 4.67%, 4.9% and 5.6%, respectively. Larger differences were found with the results of Dillon et al.,[10] with discrepancies of 47.1% at 298 K. Because k values calculated within the TST frame can be considered as an upper limit of the rate coefficient, our results seem to support the values proposed in refs 7−9. The excellent agreement with the experimental data in those references supports the validity of the proposed mechanism and of the level of theory used for both electronic and rate constant calculations.

TABLE 3: Rate Coefficients (cm^3 $molecule^{-1}$ s^{-1}) Branching Ratios (Γ) and Fractions of Conformers I and II, within the Temperature Range 280−500 K

T (K)	$10^{12}k_{\mathrm{I}}$	$10^{12}k_{\mathrm{II}}$	p_{I}	p_{II}	$10^{12}k_{\mathrm{overall}}$	Γa	Γb	Γc
280	3.43	7.26	0.95	0.05	3.62	0.2	99.7	0.1
290	3.16	6.37	0.95	0.05	3.34	0.2	99.7	0.1
298.15	2.98	5.79	**0.94**	**0.06**	3.15	**0.2**	**99.7**	**0.1**
300	2.95	5.67	0.94	0.06	3.11	0.2	99.7	0.1
310	2.77	5.11	0.93	0.07	2.92	0.2	99.6	0.2
320	2.62	4.65	0.93	0.07	2.76	0.2	99.6	0.2
330	2.49	4.28	0.92	0.08	2.63	0.3	99.6	0.2
340	2.39	3.96	0.92	0.08	2.52	0.3	99.5	0.2
350	2.30	3.70	0.91	0.09	2.42	0.3	99.5	0.2
360	2.23	3.48	0.91	0.09	2.35	0.3	99.4	0.2
380	2.12	3.14	0.90	0.10	2.22	0.4	99.3	0.3
400	2.04	2.89	0.89	0.11	2.14	0.5	99.2	0.3
420	1.99	2.70	0.88	0.12	2.08	0.5	99.1	0.3
440	1.96	2.57	0.87	0.13	2.04	0.6	99.0	0.4
460	1.95	2.46	0.86	0.14	2.02	0.6	98.9	0.4
480	1.95	2.39	0.85	0.15	2.02	0.7	98.8	0.5
500	1.97	2.34	0.84	0.16	2.03	0.8	98.7	0.5

According to the results shown in Table 3, the H abstractions occur almost exclusively from the $-CH_2$ sites for the whole range of studied temperatures. The contribution from the minor channels together goes from 0.3% at 280 K to 1.3% at 500 K. The prediction of channel b as the major one is in agreement with the estimations from structure−activity relationships (SAR)[45,46] and with recent experimental results reported by Butkovskaya et al.[47] However, the data reported in the present work seem to underpredict the importance of channels a and c. At 298 K, the Γ_{b} value from the results in the present work is 0.3%, versus 6−10% and 18% from SAR and ref 47, respectively. In addition, the contribution of the less stable conformer to the overall rate coefficient seems to be relevant to the proper description of the modeled system. Even though there is a very small population of the OO-*s*-trans conformer (II), the contribution of the term $p_{\mathrm{II}}k_{\mathrm{II}}$ to the overall rate coefficient is not negligible. Inclusion of this term is especially relevant as the temperature increases because its fraction becomes larger. Thus, neglecting this term would affect the values of the overall rate coefficient as well as the Arrhenius and Kooij parameters.

The tunneling corrections corresponding to each modeled abstraction channel are reported in Table 4. Abstractions from the OH group (channels Ic and IIc) are appreciably larger than those corresponding to abstractions from the $-CH_3$ and $-CH_2$ sites, for both conformers, as it was expected from the barriers of reaction. For the abstractions from the other two sites, the tunneling is smaller but yet important enough to be taken into account. Because the barrier heights are very important in the tunneling calculations, the inclusion of the reactant complex seems to be vital to reproduce the experimental data.

The influence of temperature on the overall rate coefficient within the range 280 360 K has been interpreted in terms of the Arrhenius equation,[48] to compare with the experimental data recently reported by Dillon et al.[10] This equation can be written as

$$k = A\mathrm{e}^{-E_{\mathrm{a}}/RT} \tag{10}$$

where A is known as the preexponential factor or the frequency

TABLE 4: Tunneling Corrections Corresponding to All the Modeled Channels

T (K)	Ia	Ib	Ic	IIa$_{eclipsed}$	IIa$_{alternated}$	IIb	IIc
280	26.27	1.45	147.12	57.28	19.75	3.48	115.52
290	20.17	1.38	103.42	41.87	15.84	3.15	83.94
298.15	**16.61**	**1.33**	**79.52**	**33.21**	**13.46**	**2.92**	**66.09**
300	15.94	1.32	75.13	31.60	12.99	2.88	62.75
310	12.91	1.27	56.20	24.53	10.86	2.65	48.11
320	10.69	1.22	43.16	19.52	9.23	2.46	37.74
330	9.01	1.18	33.92	15.87	7.96	2.29	30.21
340	7.73	1.14	27.22	13.16	6.95	2.15	24.63
350	6.72	1.11	22.25	11.10	6.14	2.03	20.41
360	5.92	1.08	18.50	9.51	5.49	1.92	17.17
380	4.75	1.03	13.35	7.25	4.49	1.74	12.63
400	3.94	1.00	10.11	5.77	3.79	1.60	9.70
420	3.36	1.00	7.97	4.75	3.27	1.49	7.73
440	2.93	1.00	6.48	4.02	2.87	1.40	6.34
460	2.60	1.00	5.42	3.47	2.57	1.32	5.33
480	2.35	1.00	4.63	3.06	2.33	1.25	4.57
500	2.14	1.00	4.03	2.74	2.13	1.19	4.00

factor and E_a represents the activation energy. In eq 10 the influence of the temperature is accounted for in the exponential part of the expression.

As can be seen in Figure 7, the Arrhenius plot corresponding to $k_{overall}$ is significantly curved. Consequently, the activation energy changes in the temperature range 280−500 K. In such cases, the procedure most commonly used to analyze the data when the plot of ln *k* versus 1/*T* is not linear, is to use the equation proposed by Kooij:[49]

$$k = BT^m e^{-E_0/RT} \tag{11}$$

where *B*, E_0 and *m* are temperature independent parameters. This expression is more satisfactory than eq 10, from both the theoretical and empirical points of view. Even data that show significant deviations from the Arrhenius equation can usually be fitted very well by eq 11. Its applicability can be tested by plotting ln(k/T^m) vs 1/*T*. If a straight line is obtained, its slope is equal to $-E_0/R$, and E_0 can be calculated. Differentiation of eq 11 in its logarithmic form leads to

$$\frac{d \ln k}{dT} = \frac{E_0 + mRT}{RT^2} \tag{12}$$

and the activation energy can be calculated, at each temperature, as

$$E_a = E_0 + mRT \tag{13}$$

where E_0 is the hypothetical activation energy at 0 K.

In our case, a plot of ln(k/T^m) vs 1/*T* yields a straight line, with R^2 equal to 0.9999, thus proving the applicability of the procedure that has been used to describe the influence of the temperature on the rate coefficient. The Kooij parameters that best fit the data are shown in Table 5. They were obtained by nonlinear square analysis. Because the starting values are of great importance in such procedure, we have obtained them by following the suggestions in ref 50 for a similar function. We have performed a multiple regression analysis, assuming ln *T* and 1/*T* as independent variables, because there is no multicollinearity among them, and ln *k* as the dependent variable. The values of E_0, *m* and *B* obtained that way were then used as the starting values in the nonlinear square analysis, leading to the final values reported in Table 6. Because none of the three parameters was fixed and the nonlinear analysis led to an R^2 coefficient of 0.999 98, the values obtained here seem to be reliable. In our opinion, the procedure described here is more reliable than that which fixes *m*, usually using $m = 2$, which can lead to different values of E_0, *m* and *B*, depending on the *m* value.

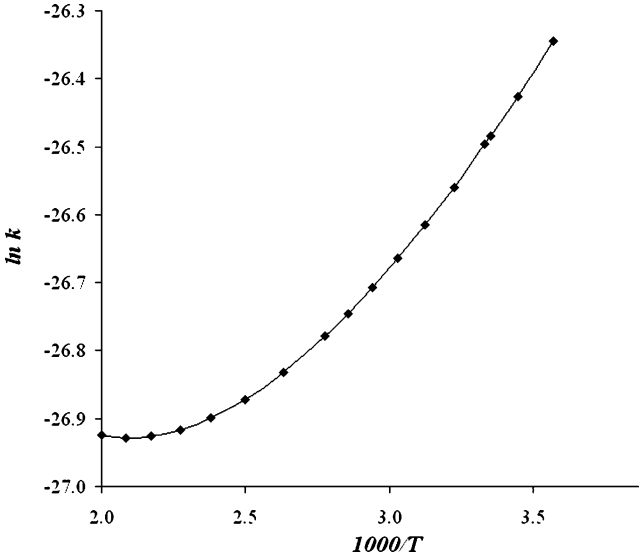

Figure 7. Arrhenius plot or the overall rate coefficient in the temperature range 280−500 K.

TABLE 5: Arrhenius and Kooij Parameters in the 280−360 and 280−500 K Temperature Ranges, Respectively[a]

parameters	overall reaction
Arrhenius (280−360 K)	
A (cm^3 molecule^{-1} s^{-1})	5.09×10^{-13}
E_a (kcal/mol)	−1.08
Kooij (280−500 K)	
B (cm^3 molecule^{-1} s^{-1})	5.29×10^{-23}
m	3.40
E_0 (kcal/mol)	−3.22

[a] Note: In this table E_0 and E_a are reported in kcal/mol, whereas in the *k* expressions in the text they appear in cal/mol.

TABLE 6: Variation of the Activation Energies (kcal/mol) with Temperature, in the 280−500 K Range

T (K)	E_a (overall)
280	−1.33
290	−1.27
298.15	−1.21
300	−1.20
310	−1.13
320	−1.06
330	−1.00
340	−0.93
350	−0.86
360	−0.79
380	−0.66
400	−0.52
420	−0.39
440	−0.25
460	−0.12
480	0.02
500	0.15

It could be interesting to discuss the variation of the activation energy with temperature (Table 6). The Kooij overall activation energy is negative in the whole range studied, and it increases as temperature rises. It goes from −1.33 kcal/mol at 280 K to 0.15 kcal/mol at 500 K. At 298 K, it is close to the one obtained using the Arrhenius approach: E_a(Arrhenius) = −1.08 kcal/mol and E_a(Kooij) = −1.21 kcal/mol. The two and three parameters equations for the overall reaction are $k_{overall}^{280-360} =$

$5.09 \times 10^{-13} e^{545/T}$ cm^3 molecule^{-1} s^{-1} and $k_{overall}^{280-500} = 5.29 \times 10^{-23} T^{3.4} e^{1623/T}$ cm^3 molecule^{-1} s^{-1}, respectively.

Conclusions

The OH abstraction reaction from hydroxyacetone has been modeled according to a complex mechanism involving the formation of a reactant complex in the entrance channel and of a product complex in the exit channel. Two conformers have been considered in the modeling and, for each of them, H abstractions from three possible sites have been computed: (a) $-CH_3$, (b) $-CH_2$, and (c) $-OH$. For the OO-*s*-trans conformer, two different paths were found corresponding to abstractions from the methyl group, depending on the relative position of the H to be abstracted with respect to the O in the carbonyl group: *eclipsed* and *alternated*.

The abstraction from the $-CH_2$ site was found to be dominant within the whole temperature range, varying from 99.7% at 280 K to 98.7% at 500 K. The calculated overall rate coefficient ($k_{overall}$) was found to be equal to 3.15×10^{-12} cm^3 molecule^{-1} s^{-1}, at 298 K. This value is in excellent agreement with the values previously reported by Dagaut et al.,[7] Orlando et al.,[8] and Chowdhury et al.,[9] and is twice smaller than that reported by Dillon et al.[10]

The temperature dependence of the overall rate coefficient is best fitted by the expressions $k_{overall}^{280-360} = 5.09 \times 10^{-13}\ e^{545/T}$ cm^3 molecule^{-1} s^{-1} and $k_{overall}^{280-500} = 5.29 \times 10^{-23}\ T^{3.40}\ e^{609/T}$ cm^3 molecule^{-1} s^{-1}, corresponding to the Arrhenius and Kooij approaches, respectively. The activation energy changes with temperature from -1.33 kcal/mol at 280 K to 0.15 kcal/mol at 500 K.

Acknowledgment. The author thanks the Computing Center of the Instituto Mexicano del Petróleo (IMP) for supercomputer time on SGI Origin 3000. The author also thanks professors W. T. Duncan, R. L. Bell and T. N. Truong for providing The Rate program through Internet.

References and Notes

(1) Tuazon, E. C.; Atkinson, R. *Int. J. Chem. Kinet*. **1989**, *21*, 1141.
(2) Tuazon, E. C.; Atkinson, R. *Int. J. Chem. Kinet*. **1990**, *22*, 591.
(3) Atkinson, R.; Baulch, D. L.; Cox, R. A.; Hampson, R. F., Jr.; Kerr, J. A.; Rossi, M. J.; Troe, J. *J. Phys. Chem. Ref. Data* **1999**, *28*, 191.
(4) Galano, A.; Alvarez-Idaboy, J. R.; Ruiz-Santoyo, Ma. E.; Vivier-Bunge, A. *J. Phys. Chem. A* **2005**, *109*, 169.
(5) Galano, A.; Alvarez-Idaboy, J. R.; Ruiz-Santoyo, M. E.; Vivier-Bunge, A. *ChemPhysChem* **2004**, *5*, 1379.
(6) Williams, J.; Pöschl, U.; Crutzen, P. J.; Hansel, A.; Holzinger, R.; Warneke, C.; Lindinger, W.; Lelieveld, J. *J. Atmos. Chem*. **2001**, *38*, 133.
(7) Dagaut, P.; Liu, R.; Wallington, T. J.; Kurylo, M. J. *J. Phys. Chem*. **1989**, *93*, 7838.
(8) Orlando, J. J.; Tyndall, G. S.; Fracheboud, J. M.; Estupiñan, E. G.; Haberkorn, S.; Zimmer, A. *Atmox. Environ.* **1999**, *33*, 1621.
(9) Chowdhury, P. K.; Upadhyaya, H. P.; Naik, P. D.; Mittal, J. P. *Chem. Phys. Lett*. **2002**, *351*, 201.
(10) Dillon, T. J.; Horowitz, A.; Hölscher, D.; Crowley, J. N.; Vereeckenb, L.; Peetersb, J. *Phys. Chem. Chem. Phys.* **2006**, *8*, 236.
(11) Mora-Diez, N.; Alvarez-Idaboy, J. R.; Boyd, R. J. *J. Phys. Chem. A* **2001**, *105*, 9034.
(12) Alvarez-Idaboy, J. R.; Galano, A.; Bravo-Pérez, G.; Ruiz-Santoyo, Ma. E. *J. Am. Chem. Soc*. **2001**, *123*, 8387.
(13) Bravo-Perez, G.; Alvarez-Idaboy, J. R.; Cruz-Torres, A.; Ruiz, M. E. *J. Phys. Chem. A* **2002**, *106*, 4645.
(14) Galano, A.; Alvarez-Idaboy, J. R.; Ruiz-Santoyo, Ma. E.; Vivier-Bunge, A. *J. Phys. Chem. A* **2002**, *106*, 9520.
(15) Galano, A.; Alvarez-Idaboy, J. R.; Bravo-Perez, G.; Ruiz-Santoyo, Ma. E. *Phys. Chem. Chem. Phys*. **2002**, *4*, 4648.
(16) Galano, A.; Cruz-Torres, A.; Alvarez-Idaboy, J. R. *J. Phys. Chem. A* **2006,** *110*, 1917.
(17) Alvarez-Idaboy, J. R.; Cruz-Torres, A.; Galano, A.; Ruiz-Santoyo, Ma. E. *J. Phys. Chem. A* **2004**, *108*, 2740.
(18) Alvarez-Idaboy, J. R.; Mora-Diez, N.; Boyd, R. J.; Vivier-Bunge, A. *J. Am. Chem. Soc*. **2001**, *123*, 2018.
(19) Alvarez-Idaboy, J. R.; Mora-Diez, N.; Vivier-Bunge, A. *J. Am. Chem. Soc*. **2000**, *122*, 3715.
(20) Aloisio, S.; Francisco, J. S. *J. Phys. Chem. A* **2000**, *104*, 3211.
(21) Vasvári, V.; Szilágyi, I.; Bencsura, A.; Dóbe, S.; Berces, T.; Henon, E.; Canneaux, S.; Bohr, F. *Phys. Chem. Chem. Phys.* **2001**, *3*, 551.
(22) Henon, E.; Canneaux, S.; Bohra, F.; Dóbe, S. *Phys. Chem. Chem. Phys*. **2003**, *5*, 333.
(23) Yamada, T.; Taylor, P. H.; Goumri, A.; Marshall, P. *J. Chem. Phys.* **2003**, *119*, 10600.
(24) Smith, I. W. M.; Ravishankara, A. R. *J. Phys. Chem. A* **2002**, *106*, 4798.
(25) Loomis, R. A.; Lester, M. I. *J. Chem. Phys.* **1995**, *103*, 4371.
(26) Lester, M. I.; Pond, B. V.; Anderson, D. T.; Harding, L. B.; Wagner, A. F. *J. Chem. Phys.* **2000**, *113*, 9889.
(27) Tyndall, G. S.; Orlando, J. J.; Wallington, T. J.; Hurley, M. D. *Phys. Chem. Chem. Phys.* **2002**, *4*, 2189.
(28) Frisch, M. J.; Trucks, G. W.; Schlegel, H. B.; Scuseria, G. E.; Robb, M. A.; Cheeseman, J. R.; Zakrzewski, V. G.; Montgomery, J. A., Jr.; Stratmann, R. E.; Burant, J. C.; Dapprich, S.; Millam, J. M.; Daniels, A. D.; Kudin, K. N.; Strain, M. C.; Farkas, O.; Tomasi, J.; Barone, V.; Cossi, M.; Cammi, R.; Mennucci, B.; Pomelli, C.; Adamo, C.; Clifford, S.; Ochterski, J.; Petersson, G. A.; Ayala, P. Y.; Cui, Q.; Morokuma, K.; Malick, D. K.; Rabuck, A. D.; Raghavachari, K.; Foresman, J. B.; Cioslowski, J.; Ortiz, J. V.; Stefanov, B. B.; Liu, G.; Liashenko, A.; Piskorz, P.; Komaromi, I.; Gomperts, R.; Martin, R. L.; Fox, D. J.; Keith, T.; Al-Laham, M. A.; Peng, C. Y.; Nanayakkara, A.; Gonzalez, C.; Challacombe, M.; Gill, P. M. W.; Johnson, B.; Chen, W.; Wong, M. W.; Andres, J. L.; Gonzalez, C.; Head-Gordon, M.; Replogle, E. S.; Pople, J. A. *Gaussian 98*, revision A.3; Gaussian Inc.: Pittsburgh, PA, 1998.
(29) Eyring, H. *J. Chem. Phys.* **1935**, *3*, 107.
(30) Truhlar, D. G.; Hase, W. L.; Hynes, J. T. *J. Phys. Chem.* **1983**, *87*, 2664.
(31) Duncan, W. T.; Bell, R. L.; Truong, T. N. *J. Comp Chem.* **1998**, *19*, 1039.
(32) Eckart, C. *Phys. Rev*. **1930**, *35*, 1303.
(33) Truong, T. N.; Truhlar, D. G. *J. Chem. Phys*. **1990**, *93*, 1761.
(34) Truong, T. N. *J. Phys. Chem. B* **1997**, *101*, 2750.
(35) Truong, T. N.; Duncan, W. T.; Tirtowidjojo, M. *Phys. Chem. Chem. Phys.* **1999**, *1*, 1061.
(36) Truhlar, D. G.; Isaacson, A. D.; Skodje, R. T.; Garrett, B. C. *J. Phys. Chem*. **1982**, *86*, 2252.
(37) Masgrau, L.; González-Lafont, A.; Lluch, J. M. *J. Phys. Chem. A* **2002**, *106*, 11760.
(38) Bader, R. F. W. *Atoms in Molecules − A Quantum Theory*, Oxford University Press: Oxford, 1990.
(39) Bader, R. F. W.; MacDougall, P. J.; Lau, C. D. *J. Am. Chem. Soc*. **1984**, *106*, 1594.
(40) Singleton, D. L.; Cvetanovic, R. J. *J. Am. Chem. Soc*. **1976**, *98*, 6812.
(41) Pilling, M. J.; Seakins, P. W. *Reaction Kinetics*; Oxford University Press: New York, 1996.
(42) Robinson, P. J.; Holbrook, K. A. *Unimolecular Reactions*; Wiley-Interscience: London, 1972.
(43) Jacox, M. E. *Vibrational and Electronic Energy Levels of Polyatomic Transient Molecules*; NIST: Gaithersburg, MD, 1998: Vol. 69, p 945.
(44) Ayala, P. Y.; Schlegel, H. B. *J. Chem. Phys.* **1998**, *108*, 2314.
(45) Atkinson, R. *Chem. Rev*. **1986**, *86*, 69.
(46) Atkinson, R. *Int. J. Chem Kinet*. **1987**, *19*, 799.
(47) Butkovskaya, N. I.; Pouvesle, N.; Kukui, A.; Mu, Y.; Le Bras, G. *J. Phys. Chem. A* **2006**, *110*, 6833.
(48) Arrhenius, S. *Z. Phys. Chem*. **1889**, *4*, 226.
(49) Kooij, D. M. *Z. Phys. Chem.* **1893**, *12*, 155.
(50) Draper, N. R.; Smith, H. *Applied Regression Analysis*; John Wiley & Sons: New York, 1966; Chapter 10, p 458.